Physics of a two-dimensional electron gas with cold atoms in non-Abelian gauge potentials

Indubala I. Satija,[1,2] Daniel C. Dakin,[3,1] J. Y. Vaishnav,[2] and Charles W. Clark[2]

[1]*Department of Physics, George Mason University, Fairfax, Virginia 22030, USA*
[2]*Joint Quantum Institute, National Institute of Standards and Technology, Gaithersburg, Maryland 20899, USA*
[3]*Optical Air Data Systems, 10781 James Payne Court, Manassas, Virginia 20110, USA*

Motivated by the possibility of creating non-Abelian fields using cold atoms in optical lattices, we explore the richness and complexity of noninteracting two-dimensional electron gases (2DEGs) in a lattice, subjected to such fields. In the continuum limit, a non-Abelian system characterized by a two-component "magnetic flux" describes a harmonic oscillator existing in two different charge states (mimicking a particle-hole pair) where the coupling between the states is determined by the non-Abelian parameter, namely, the difference between the two components of the "magnetic flux." A key feature of the non-Abelian system is a splitting of the Landau energy levels, which broaden into bands, as the spectrum depends explicitly on the transverse momentum. These Landau bands result in a coarse-grained "moth," a continuum version of the generalized Hofstadter butterfly. Furthermore, the bands overlap, leading to effective relativistic effects. Importantly, similar features also characterize the corresponding two-dimensional lattice problem when at least one of the components of the magnetic flux is an irrational number. The lattice system with two competing "magnetic fluxes" penetrating the unit cell provides a rich environment in which to study localization phenomena. Some unique aspects of the transport properties of the non-Abelian system are the possibility of inducing localization by varying the quasimomentum, and the absence of localization of certain zero-energy states exhibiting a linear energy-momentum relation. Furthermore, non-Abelian systems provide an interesting localization scenario where the localization transition is accompanied by a transition from relativistic to nonrelativistic theory.

I. INTRODUCTION

Methods for creating fields that couple to neutral atoms in the same way that electromagnetic fields couple to charged particles have created the exciting possibility of studying the effects of a generalized magnetism using cold atoms [1–3]. Using laser induced hopping, a controlled phase can be imposed upon particles moving along a closed loop in an optical lattice. The associated synthetic fields can be sufficiently strong to enter the regime of exotic magnetic phenomena that have been difficult to explore in condensed matter experiments, such as the fragmented fractal spectrum of a two-dimensional electron gas (2DEG) in a magnetic field, the famous "Hofstadter butterfly" [4]. Such fields need not obey Maxwell's equations, thus providing the possibility of discovering fundamentally new physics [5]. For example, we discuss here the generation of non-Abelian fields, by using cold atoms that occupy two Zeeman states in the hyperfine ground level [3]; these two states may be thought of as "colors" of the gauge fields, and such a system may be used to simulate lattice gauge theories in (2+1) dimensions. Other potential applications of non-Abelian fields are the creation of counterparts of magnetic monopoles [1] and integer and fractional quantum Hall effects [6].

In this paper, we adopt the 2DEG as a motif for the study of cold atom systems. The subject of 2DEGs in a magnetic field is a textbook topic [7], as the problem maps to a one-dimensional harmonic oscillator. The discrete energy levels of the oscillator are the Landau levels that describe free particle energies in terms of the quantized units $\hbar\omega_c$, where $\omega_c = eB/mc$ is the cyclotron frequency of the corresponding classical motion. Each level is highly degenerate, reflecting the fact that a classical electron spirals about a line parallel to the magnetic field, with an arbitrary center in the transverse plane. The degree of degeneracy is equal to $L^2/2\pi\delta^2$ where $\delta = \sqrt{\hbar c/eB}$ is the magnetic length and L^2 is the area of the system.

Beginning with the celebrated work of Onsager [8], Harper [9], and then Hofstadter [4], the subject of 2DEGs in a crystalline lattice in a magnetic field has fascinated physicists as well as mathematicians. In the presence of a lattice, each Landau energy level splits into Q bands, where the rational number P/Q is the magnetic flux through the unit cell in units of the magnetic flux quantum (fluxoid). The heart of the problem is the two competing periodicities related to the ratio of the reciprocal of the cyclotron frequency and the period of the motion of the electron in the periodic lattice. Two key aspects that have been explored extensively are the exotic multifractal spectrum (Hofstadter butterfly), and the metal-insulator transition obtained by tuning the ratio of the tunneling along the two directions of the lattice [9]. In contrast to Mott transition, which has its origin in particle interactions, the metal-insulator under consideration here has its origin in the irrational flux quanta penetrating the unit cell. Furthermore, unlike the Mott insulating phase which is associated with the appearance of a gap and hence is accompanied by a transition from compressible to impressible state, localization transition induced by competing periodicities is characterized by exponential decay of the single particle wave function.

This paper revisits the metal-insulator transition when the 2DEG is subjected to a non-Abelian gauge field which is a natural generalization of the uniform magnetic field. Such fields yield a much richer spectral and transport landscape

than is encountered in the Abelian case. Recent studies have shown that this transition can be demonstrated using ultracold atoms in an artificial magnetic field [2,10].

The generic experimental setup for producing non-Abelian U(2) gauge fields that we consider here, consists of a two-dimensional optical lattice populated with cold atoms that occupy two hyperfine states [2,3]. Such systems exhibit three competing length scales, associated with two distinct "magnetic fluxes" (denoted by α_1 and α_2) that penetrate the unit cell. Our aim is to describe some of the generic properties of such systems. Although our main focus is on optical lattices, we first discuss the corresponding continuum problem, where the infinite degeneracy of the Landau levels is lifted by non-Abelian interactions. The continuum problem mirrors some of the features subsequently encountered in the lattice system.

In the discussion of the metal-insulator transition in the lattice, we focus on the ground state as well as the states at the band center. These two cases are relevant for experimental systems involving Bose condensates and fermionic gases near half-filling, respectively. Some of these results were described in an earlier paper [11]. In addition to a detailed analysis, here we describe new results, such as the simulation of relativistic phenomena using cold atoms in non-Abelian fields. By tuning lattice anisotropy, we can implement relativistic as well as nonrelativistic dynamics, with a particular focus on the effects of disorder. Simulation and detection of Dirac fermions using single-component cold atoms in a hexagonal lattice was recently proposed [12]. The systems we propose here provide the possibility of observing relativistic particles and also of studying their localization properties. We show that the non-Abelian systems provide an experimental realization of the defiance of localization by disordered relativistic fermions, a topic that has been the subject of extensive study [13].

In Sec. II, we introduce non-Abelian gauge fields and the corresponding effective "magnetic fields." Section III examines the continuum limit of a single particle in a non-Abelian gauge field. In Sec. IV, we discuss lattice systems subjected to these fields, and describe methods of calculation. In Sec. V, we study various spectral characteristics of the non-Abelian lattice systems. There, following long established practice for studying metal-insulator transition in Abelian systems, we fix $\alpha_1 = (\sqrt{5}-1)/2$, the golden mean, which we denote as γ. The irrationality of α_1 ensures the existence of a localization transition [9,14]. For α_2, we consider a selected set of both rational and irrational values.

Sections VI and VII discuss localization properties of the states at the band center ($E=0$) and at the band edge. The localization of the $E=0$ states brings out some of the most important features of the non-Abelian cases, including the dependence of the transition upon a conserved momentum. Furthermore, a unique aspect of the non-Abelian system, namely, the defiance of localization of the $E=0$ states, emerges when the energy-momentum relation mimics the behavior of relativistic particles. Section VIII describes the experimental realization of the metal-insulator transition in cold atom lattices.

II. NON-ABELIAN GAUGE FIELDS

Effective non-Abelian vector potentials arise naturally in systems where the atoms have N degenerate internal states. The most general vector potential couples the states, and thus gives rise to a U(N) gauge symmetry. We here consider the case where $N=2$. In our treatment of the non-Abelian case, we follow the convention of an earlier study [3], adopting its form of vector potential

$$\vec{A} = \frac{\hbar c}{ea}\left(\frac{\pi}{2}\begin{pmatrix} -1 & 1 \\ 1 & -1 \end{pmatrix}, \ 2\pi\frac{x}{a}\begin{pmatrix} \alpha_1 & 0 \\ 0 & \alpha_2 \end{pmatrix}, 0\right). \quad (1)$$

The α_i determine the "magnetic fluxes" of the lattice with lattice constant a. Equation (1) is in the Landau gauge $\vec{A}(x,y) = (A_x, A_y(x), 0)$, where A_x is a constant and A_y depends only on x.

We rewrite the vector potential in terms of Pauli matrices σ_i, separating the Abelian and the non-Abelian parts of the gauge field

$$\vec{A} = \frac{\hbar c}{ea}\left[-\frac{\pi}{2}(I - \sigma_x)\hat{\mathbf{x}} + 2\pi\frac{x}{a}\alpha I\hat{\mathbf{y}} + \Delta\frac{x}{a}\sigma_z\hat{\mathbf{y}} \right], \quad (2)$$

where we have defined quantities $\alpha = (\alpha_1 + \alpha_2)/2$ and $\Delta = \pi(\alpha_1 - \alpha_2)$. Here σ_a, $a = x, y, z$ denotes Pauli matrices. The parameter Δ characterizes the non-Abelian feature of the system.

For non-Abelian fields, the effective "magnetic field" is given by

$$\hat{\mathbf{B}} = \nabla \times \hat{\mathbf{A}} - \frac{ie}{\hbar c}\hat{\mathbf{A}} \times \hat{\mathbf{A}}. \quad (3)$$

The origin of the extra term $\hat{\mathbf{A}} \times \hat{\mathbf{A}}$ can be traced to the commutator for the generalized velocity operator ($p - \frac{e}{c}A$)/M,

$$[v_n, v_m] = \frac{\hbar e}{M^2 c}\left(\partial_n A_m - \partial_m A_n - \frac{ie}{\hbar c}[A_n, A_m] \right) = \frac{i\hbar e}{M^2 c}\epsilon_{mnr}B_r.$$

For the vector potential in Eq. (1), this gives

$$\hat{B}_z = \hat{B}_0 + \Delta\left(\frac{\hbar c}{ea^2} \right)\left(\hat{\sigma}_z - \pi\frac{x}{a}\hat{\sigma}_y \right), \quad (4)$$

where $B_0 = 2\pi\alpha(\frac{\hbar c}{ea^2})$. Thus, $\alpha = B_0 a^2/(2\pi\hbar c/e)$ describes the Abelian flux quanta penetrating per unit cell of the lattice. The non-Abelian gauge potential generates a nonuniform magnetic field, as $\hat{\mathbf{B}}$ depends explicitly on the spatial coordinate x when $\Delta \neq 0$.

III. CONTINUUM LIMIT OF THE NON-ABELIAN SYSTEM

We now consider the continuum limit of the non-Abelian problem. Although the $\hat{\mathbf{A}}$ of Eq. (2) is ill defined in the continuum limit $a \rightarrow 0$, the study is useful in illustrating some key aspects of the non-Abelian systems. In general, continuum problems can also be experimentally realized, as in Ref. [1].
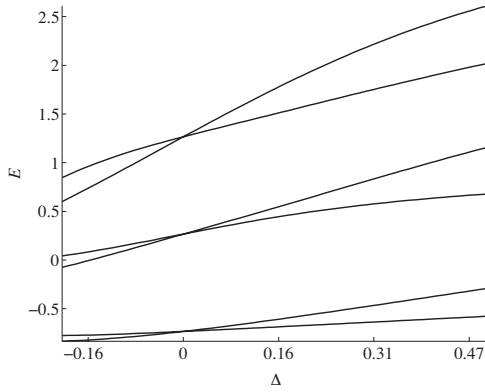
FIG. 1. Six lowest energy levels of the continuum non-Abelian Hamiltonian in Eq. (5), $\beta = \pi/2$, $M = 1$, $k_y = 1$, and $2\pi\alpha_1 = 1$. The levels are equally spaced in (and only in) the Abelian case $\Delta = 0$, where the system reduces to two decoupled harmonic oscillators.

It can be shown, after some algebra, that the two-component continuum Hamiltonian $\hat{\mathbf{H}}_c = (\hat{\mathbf{p}} - \frac{e}{c}\hat{\mathbf{A}})^2/(2M)$ resulting from the vector potential in Eq. (2) is gauge equivalent to

$$\hat{\mathbf{H}} = \frac{1}{2M}\begin{pmatrix} (\hat{p}_x + \beta)^2 + V(x) & C\Delta(x - x_0)^2 \\ C\Delta(x - x_0)^2 & (\hat{p}_x - \beta)^2 + V(x) \end{pmatrix} \quad (5)$$

up to a k_y-dependent term. The transverse momentum k_y is a conserved quantity as the Hamiltonian $\hat{\mathbf{H}}_c$ with $\vec{A}$ given by Eq. (2) is cyclic in y. Here, $\beta = \frac{\hbar\pi}{2a}$, $C = 8\pi^2\alpha(\beta/a)^2$, $V(x) = M^2\omega^2x^2/2$ with $\omega = \frac{2\pi\beta}{ma}\sqrt{(\alpha_1^2 + \alpha_2^2)/2}$ and $x_0 = 2\pi a\frac{\hbar k_y\beta}{M^2\omega^2a}\frac{\alpha_1\alpha_2}{\alpha}$. This particular form of the Hamiltonian provides an illuminating picture of the non-Abelian problem; the particle behaves as a two-component harmonic oscillator existing in a positive as well as a negative charge state. The physics of this system is that of a particle-hole pair, with the non-Abelian parameter Δ, governing the coupling between states.

The spectrum of $\hat{\mathbf{H}}_c$ is obtained by numerical diagonalization in a basis of harmonic oscillator wave functions with frequency ω. Figure 1 shows the six lowest energy levels. For fixed k_y, at $\Delta = 0$, each Landau level is twofold degenerate. For $\Delta \neq 0$ the degeneracy is lifted and the eigenstates become superposition states of a particle-hole pair.

As Fig. 1 shows, the energy levels are equally spaced only for the Abelian case $\alpha_1 = \alpha_2$. We can explicitly understand the splitting of each Landau level via degenerate perturbation theory, with Δ as a small parameter and using degenerate eigenstates

$$f_1^n = e^{ik_yy}\begin{pmatrix} e^{-i\beta x}\psi_n(x) \\ 0 \end{pmatrix}, \quad f_2^n = e^{ik_yy}\begin{pmatrix} 0 \\ e^{i\beta x}\psi_n(x) \end{pmatrix},$$

where $\psi_n(x)$ are the eigenstates of the corresponding harmonic oscillator. Perturbative correction, although linear in Δ exhibits rather complicated dependence on k_y and other parameters. Figure 2 displays the perturbative splitting of the lowest Landau level and shows it to be in good agreement with the numerical results for small Δ.

Figure 3 shows the variation of the energies with k_y, obtained numerically. In highly non-Abelian cases, the energies

bear no relation to their Abelian values. Close to the Abelian limit (bottom) the energy levels are simply split around the Abelian energies. The energies oscillate with k_y, resulting in actual and avoided crossings (i.e., the Landau bands overlap). In the vicinity of the crossings, the bands exhibit a linear dispersion relation. As we shall discuss, these features reappear in the corresponding problem of the non-Abelian gauge field on an optical lattice.

Figure 4 summarizes the effects of the non-Abelian gauge potential on the lowest Landau level of the corresponding Abelian problem. The figure describes the continuum limit of the Hofstadter "moth" [3], which is the generalization of the Hofstadter "butterfly" as the underlying gauge field becomes non-Abelian. This coarse-grained "moth" illustrates the symmetry breaking feature of the non-Abelian system as it lifts the degeneracy of the corresponding Abelian problem.
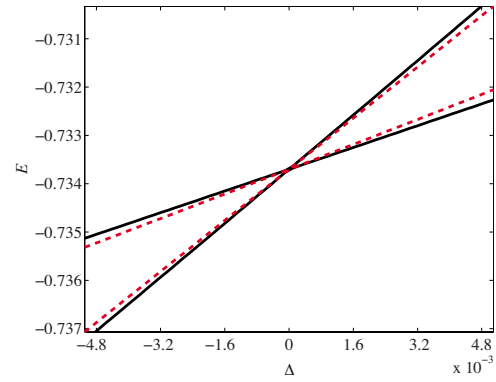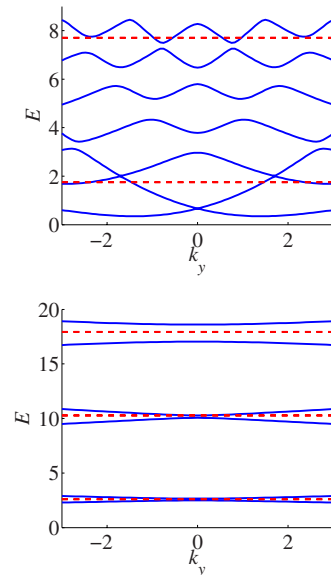

FIG. 2. (Color online) The ground-state splitting obtained numerically (see Fig. 1) (solid black), compared with that obtained by perturbation theory (dashed red) about the Abelian point $\Delta = 0$.

FIG. 3. (Color online) The three lowest energy levels of the non-Abelian system with $\alpha_1 = 1.32$ and $\alpha_2 = 0.253$ (top), $\alpha_2 = 1.11$ (bottom). The dashed line shows the Abelian levels corresponding to $\sqrt{\frac{1}{2}(\alpha_1^2 + \alpha_2^2)}$.
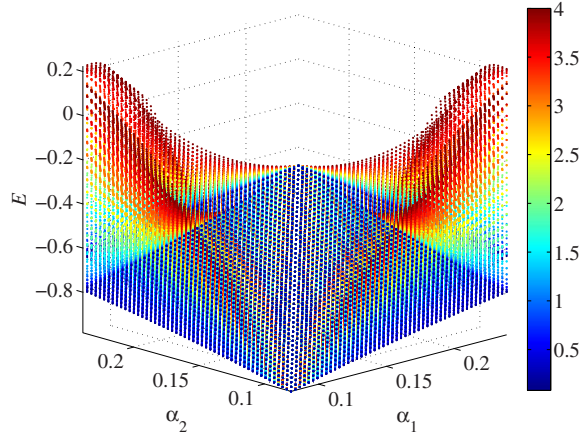
FIG. 4. (Color online) The continuum version of the Hofstadter "moth" [3]. This plot shows the energies as a function of α_1 and α_2 for a range of k_y; the color scale indicates the range of k_y. Along the line $\alpha_1 = \alpha_2$, the Abelian "backbone" of the moth, there is no k_y dependence.

IV. TWO-DIMENSIONAL LATTICE IN NON-ABELIAN GAUGE FIELDS

Our starting point is a tight binding model (TBM) of a particle moving on a two-dimensional rectangular lattice (x, y), with lattice constants (a, b) and nearest-neighbor hopping characterized by the tunneling amplitudes $(J, J\Lambda)$. When a weak external vector potential $\vec{A}(x, y) = (A_x, A_y, 0)$ is applied to the system, the Hamiltonian

$$\hat{H} = -J \left\{ \cos\left[\left(p_x - \frac{e}{c}A_x \right) \frac{a}{\hbar} \right] + \Lambda \cos\left[\left(p_y - \frac{e}{c}A_y \right) \frac{b}{\hbar} \right] \right\},$$

where $\vec{p}$ is the momentum operator. Alternatively, the Hamiltonian of a 2DEG on a lattice in the presence of a magnetic field can be written as

$$H = -\sum_{\langle ij \rangle} J_{ij} c_j^\dagger e^{i\theta_{ij}} c_i + \text{H.c.}, \tag{6}$$

where c_i is the usual fermion operator at site i. The J_{ij} is the nearest-neighbor anisotropic hopping with values J and $J\Lambda$ along the x and y directions. Throughout this paper, we will use the vector potential defined in Eq. (1).

The phase factor $\theta_{ij} = -\theta_{ji}$ defined on a link $\langle i, j \rangle$ is identified as $(2\pi e/ch)\oint \mathbf{A} \cdot \mathbf{dl}$, where $\mathbf{A}$ is the vector potential and

$$\frac{1}{2\pi} \sum_{\text{unit cell}} \theta_{ij} = e/ch \oint \mathbf{A} \cdot \mathbf{dl} = \frac{1}{\Phi_0} \oint \mathbf{B} \cdot \mathbf{dS} \tag{7}$$

is the magnetic flux penetrating the unit cell in units of magnetic flux quantum $\Phi_0 = ch/e$. We denote the eigenfunction (projected onto the x, y basis), corresponding to the eigenvalue equation $H|\Psi\rangle = E|\psi\rangle$ as $\Psi(x, y)$. With the transverse wave number of the plane wave as $\tilde{k}_y = k_y/a$, the wave function can be written as $\Psi(ma, na) = e^{i2\pi k_y n}\mathbf{g}_m$ with $x = ma$ and $y = na$.

Substituting the vector potential defined in Eq. (2), the two-component vector $\mathbf{g}_m = \binom{\theta_m}{\eta_m}$ can be shown to result in the equations

$$\begin{pmatrix} \theta_{m+1} \\ \eta_{m+1} \end{pmatrix} + \begin{pmatrix} \theta_{m-1} \\ \eta_{m-1} \end{pmatrix} - \begin{pmatrix} 0 & E - V_m \\ E - U_m & 0 \end{pmatrix} \begin{pmatrix} \theta_m \\ \eta_m \end{pmatrix} = 0,$$

where

$$U_m = 2\Lambda \cos(2\pi\alpha_1 m - 2\pi k_y),$$

$$V_m = 2\Lambda \cos(2\pi\alpha_2 m - 2\pi k_y).$$

For $\alpha_1 = \alpha_2 \pmod 1$, we recover the Abelian limit described by the Harper equation [9]

$$g_{m+1} + g_{m-1} + 2\Lambda \cos(2\pi\alpha m - 2\pi k_y)g_m = Eg_m. \tag{8}$$

For irrational values of the flux α, the system exhibits a metal-insulator transition at $\Lambda = 1$, where the model exhibits self-duality [9]. For $\Lambda < 1$, all states are extended and Bloch type while for $\Lambda > 1$, all states are exponentially localized.

The approach to the irrational values of α_i is studied by considering a sequence of periodic systems obtained by rational approximants $\alpha_i = p_i/q_i$. This corresponds to truncating the continued fractional expansion of α_1 and α_2. The resulting periodic system will have period Q, the least common multiple of q_1 and q_2.

The $2Q$-dimensional system can be cast in the form of two Q-dimensional eigenvalue problems

$$\begin{pmatrix} U_1 & 1 & 0 & 0 & . & . & . & e^{-ik_A} \\ 1 & V_2 & 1 & 0 & 0 & . & . & 0 \\ 0 & 1 & U_3 & 1 & 0 & . & . & 0 \\ 0 & 0 & 1 & V_4 & 1 & 0 & . & 0 \\ 0 & 0 & 0 & 1 & U_5 & 1 & . & 0 \\ . & . & . & . & . & . & . & . \\ e^{ik_A} & . & . & 0 & 0 & 0 & 1 & V_Q \end{pmatrix} \begin{pmatrix} \theta_1 \\ \eta_2 \\ \theta_3 \\ \eta_4 \\ . \\ . \\ . \\ \eta_Q \end{pmatrix} = E_A \begin{pmatrix} \theta_1 \\ \eta_2 \\ \theta_3 \\ \eta_4 \\ . \\ . \\ . \\ \eta_Q \end{pmatrix}$$

and

$$\begin{pmatrix} U_2 & 1 & 0 & 0 & . & . & . & e^{-ik_B} \\ 1 & V_3 & 1 & 0 & 0 & . & . & 0 \\ 0 & 1 & U_4 & 1 & 0 & . & . & 0 \\ 0 & 0 & 1 & V_5 & 1 & 0 & . & 0 \\ 0 & 0 & 0 & 1 & U_6 & 1 & . & 0 \\ . & . & . & . & . & . & . & . \\ e^{ik_B} & . & . & 0 & 0 & 0 & 1 & V_1 \end{pmatrix} \begin{pmatrix} \theta_2 \\ \eta_3 \\ \theta_4 \\ \eta_5 \\ . \\ . \\ . \\ \eta_1 \end{pmatrix} = E_B \begin{pmatrix} \theta_2 \\ \eta_3 \\ \theta_4 \\ \eta_5 \\ . \\ . \\ . \\ \eta_1 \end{pmatrix}.$$

Here E_A and E_B denote the two sets of eigenvalues of the two uncoupled systems. The allowed eigenenergies of the full system are the union of these two sets.

In the above two eigenvalue equations, we have used the Bloch condition

FIG. 5. (Color online) The two possible antiferrimagnetic states designated as A and B.

$$\begin{pmatrix} \theta_{2m-1+Q} \\ \eta_{2m+Q} \end{pmatrix} = e^{ik_A Q} \begin{pmatrix} \theta_{2m-1} \\ \eta_{2m} \end{pmatrix}, \quad \begin{pmatrix} \theta_{2m+Q} \\ \eta_{2m+1+Q} \end{pmatrix} = e^{ik_B Q} \begin{pmatrix} \theta_{2m} \\ \eta_{2m+1} \end{pmatrix}.$$

An important consequence of this decoupling of the $2Q$-dimensional problem into two Q-dimensional problems is that the eigenstates of the system are of an "antiferrimagnetic" type, as shown schematically in Fig. 5. We will refer to them as of the A and B type. The corresponding states denoted as χ_A and χ_B are, in general, nondegenerate.

It is instructive to compare the eigenvalue formulation to the transfer matrix approach discussed in earlier studies [3]. The TBM equation can be written as a transfer matrix equation

$$\begin{pmatrix} \theta_{m+1} \\ \eta_{m+1} \\ \theta_m \\ \eta_m \end{pmatrix} = T(m) \begin{pmatrix} \theta_m \\ \eta_m \\ \theta_{m-1} \\ \eta_{m-1} \end{pmatrix},$$

where

$$T(m) = \begin{pmatrix} 0 & (E-V_m) & -1 & 0 \\ (E-U_m) & 0 & 0 & -1 \\ 1 & 0 & 0 & 0 \\ 0 & 1 & 0 & 0 \end{pmatrix}.$$

The allowed energies are those for which the product of Q successive matrices $B(m)$ has an eigenvalue on the unit circle $e^{\pm i\phi_1}$ and $e^{\pm i\phi_2}$. Alternatively, the four-dimensional transfer matrix equation can be reduced to two independent two-dimensional transfer matrices as

$$\begin{pmatrix} \theta_{m+2} \\ \eta_{m+1} \end{pmatrix} = T_A(m) \begin{pmatrix} \theta_m \\ \eta_{m-1} \end{pmatrix}, \quad \begin{pmatrix} \theta_{m+1} \\ \eta_m \end{pmatrix} = T_B(m) \begin{pmatrix} \theta_{m-1} \\ \eta_{m-1} \end{pmatrix}, \quad (9)$$

where the 2×2 matrices T_A and T_B are given by

$$T_A(m) = \begin{pmatrix} (E-V_{m+1})(E-U_{m-1})-1 & -(E-V_{m+1}) \\ (E-U_m) & -1 \end{pmatrix}$$

and

$$T_B(m) = \begin{pmatrix} (E-V_m)(E-U_{m-2})-1 & -(E-U_m) \\ (E-V_{m-1}) & -1 \end{pmatrix}.$$

This decoupling of the four-dimensional transfer matrix problem into two two-dimensional transfer matrices is equivalent to the decoupling discussed earlier for the eigenvalue problem, which in turn implies the possibility of

antiferrimagnetic-type states as shown in Fig. 5. An important consequence of this type of state is that (out of four), only two of the eigenvalues of the four-dimensional transfer matrix have to be on the unit circle. In other words, in contrast to the statement made in an earlier paper [3], the allowed energies include states where two of the four eigenvalues of the transfer matrix are not on the unit circle [11].

The existence of "antiferrimagnetic" states and the relationship between the direct diagonalization method and the transfer matrix approach can be illustrated by considering a simple non-Abelian system, namely, the one with $\alpha_1 = 1/2$ and $\alpha_2 = 0$ which can be treated analytically. Diagonalization of two independent 2×2 matrices Eq. (9) gives

$$E_A(k_A, k_y) = 2[\Lambda \cos 2\pi k_y \pm \cos k_A],$$

$$E_B(k_B, k_y) = \pm 2\sqrt{\Lambda^2 \cos^2 2\pi k_y + \cos^2 k_B}$$

and the corresponding eigenvectors

$$\chi_A = \begin{pmatrix} \pm e^{-ik_A} \\ 0 \\ 1 \\ 0 \end{pmatrix}, \quad \chi_B = \begin{pmatrix} 0 \\ e^{-ik_B} \dfrac{E/2 \pm \Lambda \cos 2\pi k_y}{\cos k_B} \\ 0 \\ 1 \end{pmatrix}.$$

In general, the A and the B states are nondegenerate. As is explicit in this example, the magnitude of the two components of the vectors are in general unequal, and hence the solutions correspond to antiferrimagnetic states. However, at $k_y = \pi/2$, the $E_A = E_B$ and the two degenerate states are antiferrimagnetic.

The spectrum can also be obtained by iterating the transfer matrix problem where the energies can be written in terms of the eigenvalues of the transfer matrix $e^{\pm i\phi_A}, e^{\pm i\phi_B}$. Comparison of the spectrum obtained by these two methods shows that $\phi_A = k_A/2$ and $\phi_B = k_B/2$.

The results of this paper were obtained using the direct diagonalization method. We shall henceforth set $\alpha_1 = \gamma$, the golden mean, and explore various complexities of the problem for different values of α_2. Here we confine ourselves to simple fractions such as 1/2, 1/3, 1/4, etc., while for the irrational case, we choose $\alpha_2 = \gamma^3, \gamma^4$. In contrast to the continuum problem, in the lattice problem, the spectral and transport properties are sensitive to number theoretical properties of α_i and hence the effects of non-Abelian feature cannot be studied by small variation in the non-Abelian parameterΔ.

V. NON-ABELIAN SPECTRUM FOR IRRATIONAL α_1

The energy spectrum of the system is the union over k_y of the individual energy spectra of the A and the B types of the tight binding equations. In the Abelian case $\alpha_1 = \alpha_2$ and when α_1 is rational, equal to p/q, the spectrum consists of q bands which are usually separated by gaps. As k_y varies, the bands shift and their width may change, but they do not overlap, except at the band edges. For irrational α, the spectrum is independent of k_y.
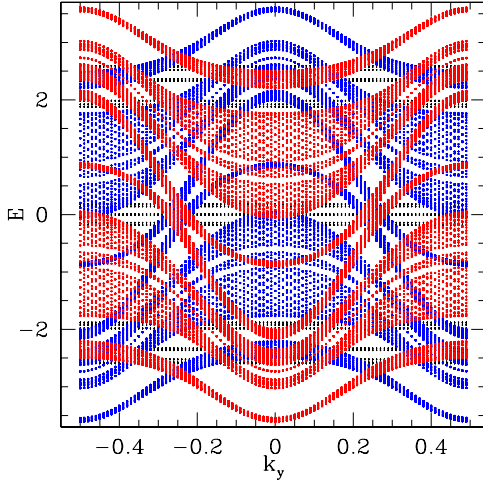
FIG. 6. (Color online) Energy spectrum viewed as a function of k_y for $\alpha_1 = 89/144$ and $\alpha_2 = \frac{1}{2}$ with $\Lambda = 1$ for a range of k_x values. Family of bands with minima (maxima) at $k_y = 0$ correspond to $E_A(E_B)$. The set of bands that show no variation with k_y describe the corresponding Abelian case with $\alpha_1 = \alpha_2 = \gamma$.

A striking aspect of the non-Abelian problem is the overlapping of the bands, as illustrated in Figs. 6 and 7. These figures depict two different classes of typical non-Abelian spectra with rational α_2: In Fig. 6, type-*A* and -*B* solutions result in a nondegenerate spectrum; and Fig. 7 shows the case where *A* and *B* solutions are degenerate. Below we discuss various spectral characteristics of the system.

For rational $\alpha_2 = p_2/q_2$, the spectrum is found to be a periodic function of k_y. We list below some of the characteristic properties of the spectrum that are observed in numerical studies: (1) $E_{A,B}(2\pi k_y) = -E_{A,B}(2\pi k_y + 2\pi\alpha_2)$, (2) $E_A(2\pi k_y) = -E_B(2\pi k_y + 2\pi\alpha_2)$, (3) $E_{A,B}(2\pi k_y) = E_{A,B}(2\pi k_y + 4\pi\alpha_2)$, (4) $E(2\pi k_y) = E(2\pi k_y + 4\pi\alpha_2)$.

For certain values of α_2, *A*- and *B*-type of states are degenerate. This happens when the two sets $V_{2m}(k_y)$ and $V_{2m+1}(-k_y)$ coincide. This degeneracy occurs when (a) α_2 is
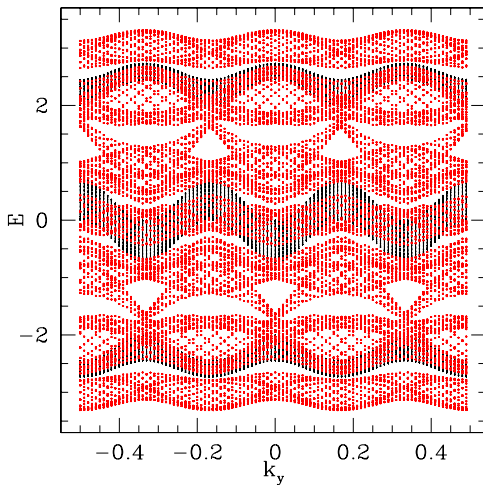

FIG. 7. (Color online) Energy spectrum viewed as a function of k_y for $\alpha_1 = 89/144$ and $\alpha_2 = \frac{1}{3}$ with $\Lambda = 0.5$. The set of nonintersecting bands show a corresponding Abelian case with $\alpha_1 = \alpha_2 = \frac{1}{3}$.

an irrational number and (b) $\alpha_2 = p/q$ with q odd as $V_{m+qn}(k_y) = V_{q-m+qn}(-k_y)$ (where n is an integer and $m < q$). For even q, the *A* and *B* states are, in general, nondegenerate. This distinction between the odd and even cases leads to significant differences between these two cases.

VI. THE LOCALIZATION TRANSITION

The metal-insulator transition [14] in 2DEGs in the presence of a magnetic (Abelian) field is a paradigm for the Anderson localization transition. We now discuss the corresponding localization transition that exists in the non-Abelian systems. In the metallic phase, the wave function is extended and its Fourier transform is characterized by sharp Bragg fringes at the reciprocal lattice vectors of the lattice. In the insulating phase the wave function is exponentially localized resulting in the broadening of the fringes.

In contrast to the Abelian case described by Harper equation, where all states localize at the same value of the tunneling anisotropy, localization in the non-Abelian case varies throughout the spectrum. In this section, we will discuss the localization properties of the $E = 0$ state a study is relevant for fermionic atoms near half-filling. As shown below, for $\alpha_2 = \frac{1}{2}$ as well as for $\alpha_2 = \frac{1}{4}$, the onset to a localization transition can be inferred from the well-known localization characteristics of the Harper equation [9].

A. Localization boundary for $\alpha_2 = 1/2$

For $\alpha_2 = \frac{1}{2}$, the coupled TBM equations [Eq. (10)] for $E = 0$ reduce to

$$\theta_{m+2} + \theta_{m-2} + 2(-1)^m \lambda \cos(2\pi\alpha_1 m - 2\pi k_y)\theta_m = \epsilon\theta_m,$$

$$\eta_{m+1} + \eta_{m-1} + 2\Lambda \cos(2\pi\alpha_1 m - 2\pi k_y)\theta_m = 0,$$

where $\epsilon = -2$ and $\lambda = 2\Lambda^2 \cos(2\pi k_y)$. For $E = 0$, the uncoupled θ equation maps to an $E = -2$ Harper-like equation (10), where the on-site quasiperiodic potential is a sinusoidal function of k_y. The eigenstates of this system localize at $\lambda = 1$, providing an explicit threshold for localization of the $E = 0$ state of the non-Abelian system provided $\epsilon = -2$ is the eigenvalue of Eq. (10).

As shown in Fig. 8, $\epsilon = -2$ is an eigenvalue of the system provided $\lambda = \lambda_1 \lesssim 0.48$ or $\lambda = \lambda_2 \gtrsim 1.83$. These critical values determine the boundary curves for the localization of the $E = 0$ state: in the Harper equation, all states are extended for values of $\lambda \leq 1$. These two localization boundaries are exhibited in Fig. 9

B. Localization boundary for $\alpha_2 = 1/4$

For $\alpha_2 = \frac{1}{4}$, the uncoupled θ equations for the *A* and the *B* sectors of the TBM for $E = 0$ reduce to

$$\bar{\theta}^A_{m+2} + \bar{\theta}^A_{m-2} + 2i\lambda_A \cos(2\pi\alpha_1 m - 2\pi k_y)\bar{\theta}^A_m = 0,$$

$$\bar{\theta}^B_{m+2} + \bar{\theta}^B_{m-2} + 2i\lambda_B \sin(2\pi\alpha_1 m - 2\pi k_y)\bar{\theta}^B_m = 0,$$
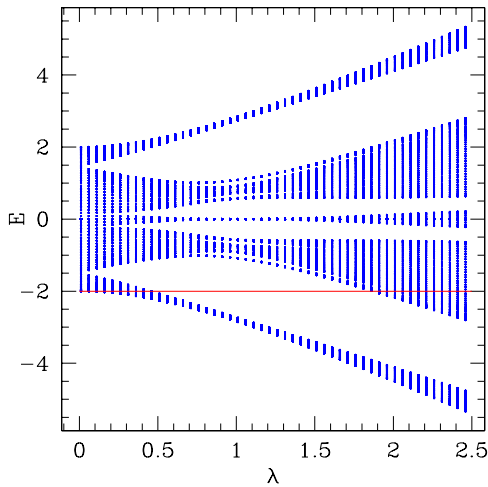
where

FIG. 8. (Color online) The eigenvalues of the effective TBM [Eq. (10)] describing $E=0$ states as λ varies. The line (red online) shows the values of λ where $E=0$ is an eigenvalue of the TBM [Eq. (10)].

$$\lambda_A = 2\Lambda^2 \cos(2\pi k_y), \quad \lambda_B = 2\Lambda^2 \sin(2\pi k_y).$$

The above two equations correspond to A- and B-type states with $E=0$, respectively. Here $\bar{\theta}_m^{A,B} = i^m \theta_m^{A,B}$. In a manner analogous to the corresponding Hermitian problem, the system exhibits self-duality at $\lambda_{A,B}=1$ and this self-dual point describes the onset of localization [15]. For $k_y = \frac{1}{8} \pmod{\frac{1}{4}}$, both types of solutions localize simultaneously. However, at other values of the transverse momentum, only one of the states is localized. This is an example of two degenerate states with different transport properties: depending upon (Λ, k_y), type-A states may be extended (localized) while type-B states will be localized (extended). This localization boundary in Λ-k_y space is shown for types A and B in Fig. 10.
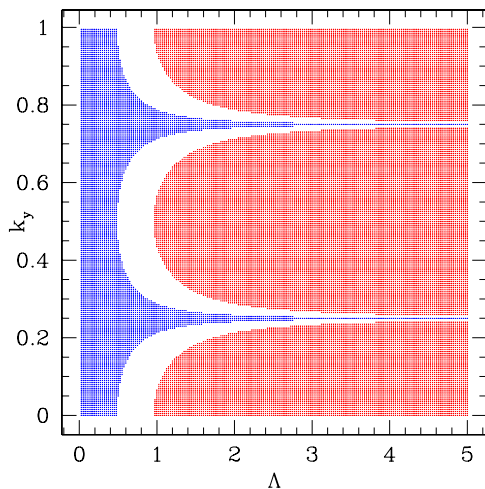

FIG. 9. (Color online) With $\alpha_2 = 1/2$ shaded regime that begins at $\Lambda=0$ shows the extended phase while shaded lobes that begin at $\Lambda=1$ and extend to all values of $\Lambda>1$ show the localized phase of $E=0$ state in the Λ-k_y plane.
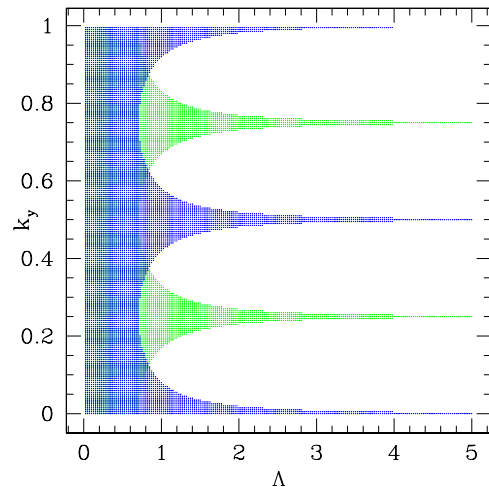

FIG. 10. (Color online) For $\alpha_2 = 1/4$, shaded regimes show extended phase for two degenerate $E=0$ states with lobes centered at $k_y = 0.25$ and $k_y = 0.75$ corresponding to A type while the rest of the regime correspond to B type.

The existence of conducting states for all values of Λ is one of the most intriguing characteristics of the non-Abelian system. Below we show that these states defying localization describe relativistic particles.

C. Relativistic dispersion and defiance of localization

Figure 11 shows the energy-momentum relation for $\alpha_2 = 1/2$ near $E=0$, $k_y = 1/4$. Although the level structure is complicated, near $k_y = 1/4$, the energy bands exhibit the linear dispersion characteristic of the one-dimensional relativistic particles. Thus, the non-Abelian system with A- and B-type states, provides an interesting manifestation of the positive and the negative energy states of a one-dimensional relativistic particle.

An important characteristic of the states that reside at the crossings is that they defy localization. It should be noted
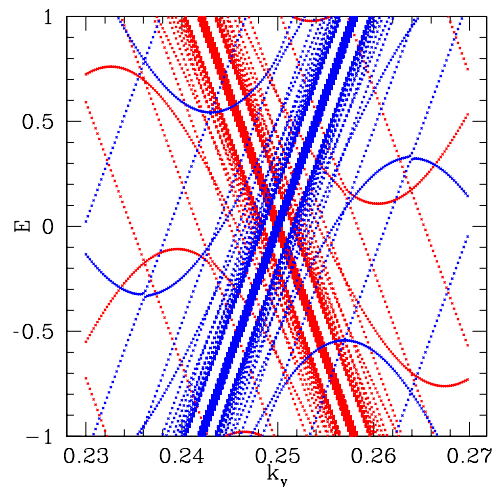

FIG. 11. (Color online) Blowup of the $E=0$ and $k_y = 1/4$ neighborhood for $\alpha_1 = 89/144$ and $\alpha_2 = \frac{1}{2}$ and $\Lambda=10$. Bands going left to right (right to left) correspond to E_a (E_b).
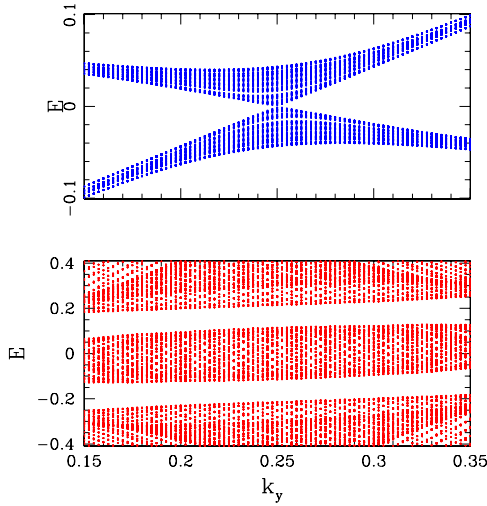
FIG. 12. (Color online) The top and bottom panels show the spectrum for $\alpha_2 = \gamma^3$ with $\Lambda = 0.75, 1.25$, respectively, which correspond to extended and localized $E=0$ states, respectively.
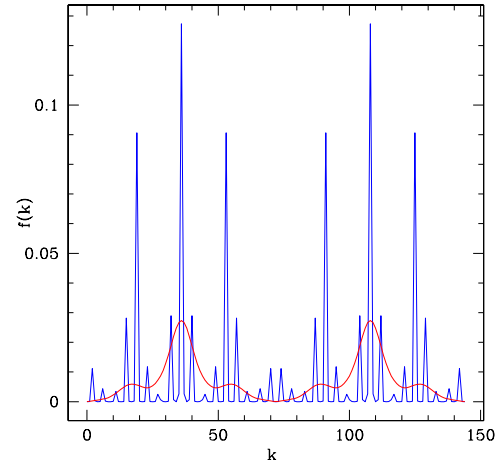

FIG. 13. (Color online) Fourier transform of the wave function for $E=0$ state with $\alpha_2 = \gamma^3$ with $\Lambda = 0.75$ (sharp fringes) and $\Lambda = 1.25$ (smeared out fringes). The label k on the x axis corresponds to the momentum $2\pi k/L$, where L is the size of the lattice.

that a crossing at $E=0$ exists irrespective of the value of Λ. In other words, we have a relativistic theory for all values of Λ as shown in Figs. 6 and 11. Such states remain extended irrespective of the quasiperiodic disorder in the system as the linear dispersion exists for the full range of Λ values.

For $\alpha_2 = \frac{1}{4}$, we obtain an effective relativistic theory for zero-energy states near $k_y = 0$ for type-A and near $k_y = \pi/2$ for type-B states. These states remain conducting for all values of Λ.

We would like to note that in the Abelian system, a linear energy-momentum relation resulting in a Dirac cone occurs for rational values of α in the neighborhood of some special values of k_x, k_y near $E=0$. However, for irrational α, the spectrum is independent of k_y and the Dirac cone disappears. Therefore, in the Abelian case, effective relativistic theory bears no relationship to the transport properties as the states are always extended for rational α.

D. Localization transition and loss of relativistic dispersion

Our detailed investigation for various values of α_2 shows that the presence of conducting states for all values of Λ is not a generic property of the system. In particular, for cases where the type-A and type-B states are always degenerate, all states are found to localize. Interestingly, the transition to localization is accompanied by a loss of the relativistic character of the energy momentum relation.

For example, for $\alpha_2 = p/q$ where q is odd, as well as for irrational α_2, the crossings characterizing certain $E=0$ states disappear beyond a certain critical value of Λ. Interestingly, this threshold for the disappearance of the crossing is always found to coincide with the onset to localization of that state. Figures 12 and 13 illustrate this for irrational α_2 as the disappearance of band crossings is accompanied by the broadening and flattening of the Bragg peaks.

VII. LOCALIZATION TRANSITION OF BOSE-EINSTEIN CONDENSATES

The natural locus for BEC in ultracold atoms in optical lattices is the band edge. We now explore the spectral and

transport properties of the states at band edges, namely, the minimum energy states as k_y varies. For very low filling factor, this is also relevant for the electron problem. In contrast to the preceding analytical treatment of the band centers, we have investigated localization properties of the states at the band edge with numerical methods.

As seen from Figs. 6 and 14, the energy spectrum for $\alpha_2 = \frac{1}{2}$ shows the existence of a linear dispersion relation near the band crossings. As the lattice anisotropy Λ varies, we see a transition from relativistic to nonrelativistic behavior near $\Lambda \approx 2.5$; this transition is accompanied by the loss of the wave function's spinor character, causing an effective spin polarization.

The robustness of the linear dispersion in non-Abelian systems is shown for various values of α_2 in Figs. 15 and 16. It appears that it is only in the even-q cases that the nature of the dispersion changes as Λ varies. Similarly, for $\alpha_2 = \gamma^4$ (an odd harmonic of γ, as $\gamma^4 = 2 - 3\gamma$), linear dispersion at k_y
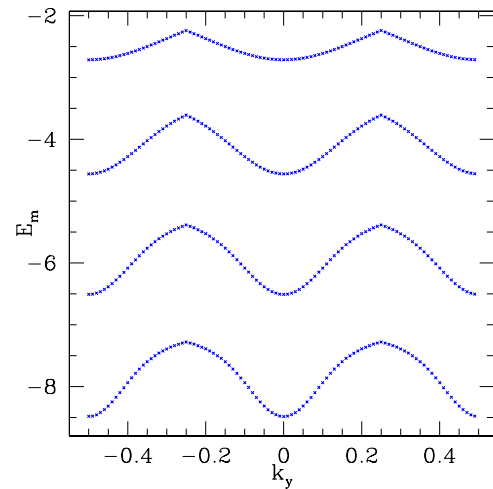

FIG. 14. (Color online) Minimum energy as a function of k_y for $\alpha_2 = \frac{1}{2}$ with $\Lambda = 0.5, 1.5, 2.5, 3.5$ (top to bottom) illustrating the change from linear to quadratic dispersion near $k_y = \pm 1/4$.
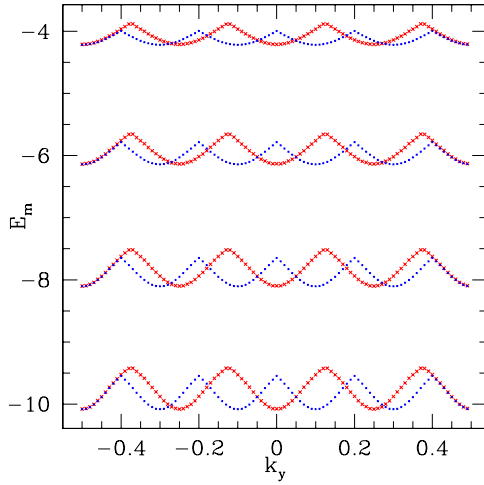
FIG. 15. (Color online) Minimum energy as a function of k_y for $\alpha_2 = 1/4$ (cross), $\alpha_2 = 1/5$ (dots) with $\Lambda = 1.5, 2.5, 3.5, 4.5$ (top to bottom) illustrating the change from the linear to quadratic dispersion near $k_y = \pm 1/4$.

$=0$ and at $k_y = 1/4$ occurs for all values of Λ, while for $\alpha_2 = \gamma^3$ (an even harmonic of γ, as $\gamma^3 = 2\gamma - 1$), a relativistic energy-momentum relation is seen for small and large values of Λ as illustrated in Fig. 16. In other words, a "transition" from relativistic to nonrelativistic behavior can be induced by varying Λ for some values of α_2. Another point to be noted is that the ground state of the system may have non-zero momentum: for even q, the global energy minimum occurs at $k_y = 0$, while for odd q, it occurs at $k_y = \alpha_2/2$.

Figures 17 illustrate the localization transition of the minimum energy states. Extended states in these figures are characterized by sharp Bragg peaks in the momentum distribution, and the localization transition is signaled by the broadening of these peaks. As we increase the parameter Λ, the $k_y = \pm 1/4$ states localize before the $k_y = 0$ state. Our detailed investigation shows that $k_y = 0$ is the last state to localize as Λ is varied for all values of α_2. This is contrary to
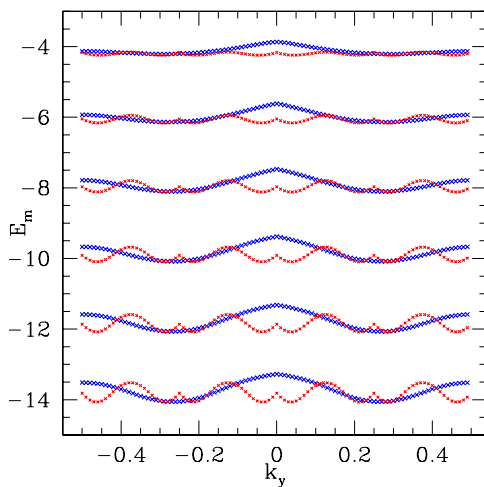

FIG. 16. (Color online) Variation of minimum energy with k_y for $\alpha_2 = \gamma^3$ (large crosses) and $\alpha_2 = \gamma^4$ (smaller crosses) with $\Lambda = 1.5, 2.5, 3.5, 4.5, 5.5, 6.5$ (top to bottom).
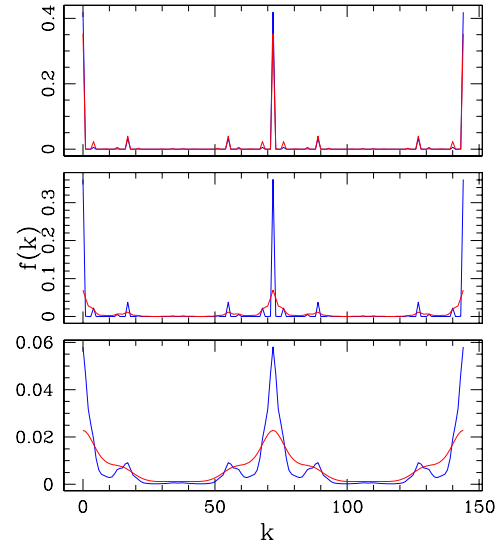

FIG. 17. (Color online) Fourier transform of the wave function for $\Lambda = 0.4, 0.5, 0.7$ (top to bottom). Each caption shows $k_y = 0.25$ (red) and $k_y = 0$ (blue) for the minimum energy state for $\alpha_2 = 1/2$. The x axis index k corresponds to the Bloch vector $2\pi k/L$. There are peaks corresponding to the irrational values of α_1, occurring at k values equal to half of the Fibonacci numbers (as antiferromagnetic nature effectively doubles the size of the unit cell). Additional satellite peaks characterize the non-Abelian feature of the system.

familiar experience, in which localization begins at the band edge. The localization for the minimum energy state is insensitive to the energy-momentum relation, in contrast to the $E = 0$ states.

For irrational α_2, we expect the localization threshold to be lowered. Our numerical results show that the minimum energy states begin to localize at a relatively small value of $\Lambda \approx 0.15$. As discussed earlier, $E = 0$ states resist localization due to their linear dispersion but eventually localize. Our numerical studies show that localization is complete at $\Lambda = 1$, as in the Abelian case.

VIII. EXPERIMENTAL OBSERVATION OF METAL-INSULATOR TRANSITION

An experimental setup for generating artificial Abelian and non-Abelian fields consists of Refs. [2,3] a two-dimensional optical lattice populated with cold atoms that occupy two hyperfine states. The lattice laser polarization is adjusted to confine these states to alternating columns. The non-Abelian scheme requires atoms with two pairs of hyperfine levels: $|g_1\rangle$, $|e_1\rangle$, $|g_2\rangle$, $|e_2\rangle$ as shown in Fig. 18.

The typical kinetic energy tunneling along the y direction is suppressed by accelerating the system or applying an inhomogeneous electric field in that direction such that the lattice is tilted. Tunneling is instead accomplished with two sets of laser-driven Raman transitions with space-dependent Rabi couplings $\Omega_j e^{iq_j y}$, where $j = 1, 2$. The wave numbers q_j generate an effective magnetic flux where $q_j = (2\pi\alpha_j)/a$, where $\lambda = 2a$ is the wavelength of the laser light. In an optical lattice with a finite number of sites, the two components of the "magnetic flux" (α_1, α_2) can be adjusted, in a controlled
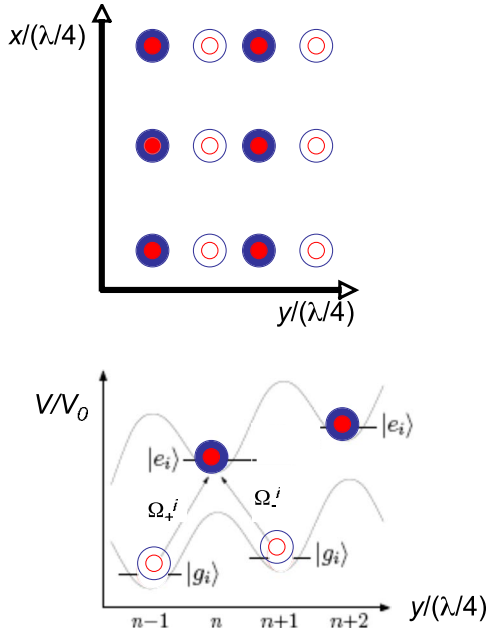
FIG. 18. (Color online) Schematic diagram illustrating the non-Abelian U(2) setup. The ground states are hollow and the excited states are filled. Red and blue represent the two "colors" of the U(2) group.

FIG. 19. (Color online) Λ as the depth of the 2D optical lattice is tuned with $\alpha = \frac{1}{2}$. The factor $E_R/\hbar\Omega \approx 4.2$ with the following laser parameters: $I_g = 1$ mW/cm^2, $\xi = 11$, $\delta_r = 100$ GHz, $E_R/h = 3.2$ kHz.

$$J_x \approx 1.397 E_R \left(\frac{V_0}{E_R}\right)^{1.051} \exp[-2.121\sqrt{V_0/E_R}]. \quad (12)$$

The ratio of $\Lambda = J_x/J_y = (E_R/\hbar\Omega)f(V_0/E_R, \alpha)$ is shown in Fig. 19 for a characteristic range of V_0/E_R with the scale set by the factor $\hbar\Omega/E_R$. In order to generate a useful range of Λ values (e.g., $0 < \Lambda \lesssim 2$), the parameter $\hbar\Omega/E_R$ must be set to order unity.

We now argue that it is possible to achieve this with reasonable experimental settings. We consider the case of ^{87}Rb, where the $|g\rangle$ and $|e\rangle$ states are taken to be the hyperfine levels of the $5^2S_{1/2}$ level [17] and the Raman level is $5^2P_{3/2}^\circ$. The parameter $\hbar\Omega/E_R$ can be fixed near unity if the Raman laser beams have intensities on the order of 1 mW/cm^2 and are detuned from the ^{87}Rb D_2 line by about $\delta_r \approx 100$ GHz. We require that the Rabi coupling of the Raman transition Ω, the detuning Δ, and the lattice trapping frequency $\nu_x = \sqrt{4E_R V_0}/\hbar$ have well separated magnitudes such that $\Omega \ll \Delta \ll \nu_x$, to ensure that only the lowest band of the lattice is occupied and no other excitations occur. Typical values of ν_x are on the order of tens of kilohertz. The Raman transition is stimulated by two lasers with Rabi couplings $\Omega_g^{(1)}$ and $\Omega_e^{(1)}$ and intensities I_g and I_e with a large detuning δ_r such that the effective Rabi coupling magnitude is $\Omega = \Omega_g^{(1)}\Omega_e^{(1)}/2\delta_r$. The Rabi coupling Ω can be written as a product of atomic factors and laser tuning parameters

$$\Omega = \left(\frac{\Gamma^2}{4I_{\text{sat}}}\right)\left(\frac{\sqrt{\xi}I_g}{\delta_r}\right),$$

where Γ is the natural decay rate of the $5^2P_{3/2}^\circ$ state and I_{sat} is the saturation intensity of the D_2 line (see Ref [17].). The ratio $\xi = I_e/I_g$ must be less than 0.17 or greater than 5.8 to satisfy the $\Omega \ll \Delta$ condition. The separation of scales between the Rabi coupling Ω of the Raman transition and lattice trapping frequency ν_x necessary to generate the magnetic field in the above scheme (i.e., $\Omega \ll \nu_x$) is sufficient to generate a reasonable range of Λ values.

In the non-Abelian case, there are generally two possible values of Λ corresponding to Ω_1 and Ω_2, one for each "color." By adjusting $\Omega_2/\Omega_1 = f(V_0/E_R, \alpha_1)/f(V_0/E_R, \alpha_2)$, we obtain a single Λ in correspondence with the theoretical studies described here.

manner, to a sequence of rational approximants to the golden mean by tuning the q_j. We direct readers to Refs. [2,3] regarding various details for generating these artificial gauge fields.

We now describe the experimental feasibility of tuning Λ to induce metal-insulator transitions by adjusting the lattice beam intensity V_0. For simplicity, we will initially discuss the Abelian case. Let us first consider the laser assisted coupling J_y as a function of V_0/E_R, where $E_R = 2\pi^2\hbar^2/M\lambda^2$ is the photon recoil energy. The tunneling is defined as the matrix element of the Rabi coupling (Ω) between Wannier functions w, evaluated at the two adjacent lattice sites

$$J_y = \int w(\vec{x} - \vec{x}_i)\frac{\hbar}{2}\Omega \exp(iqx)w(\vec{x} - \vec{x}_{i-1})d^3x, \quad (10)$$

where $q = (2\pi\alpha)/a$. The Wannier functions for $V(x) = V_0 \sin^2(2\pi x/\lambda)$ have been computed [2]; J_y decreases monotonically with V_0/E_R. This basic behavior can be demonstrated analytically by assuming a deep lattice approximated by a harmonic oscillator potential and taking the Wannier functions to have the corresponding Gaussian form. The Gaussian approximation yields

$$J_y = \frac{\hbar\Omega}{2}\exp\left[-\frac{\pi^2}{16}\sqrt{V_0/E_R}\right]\exp\left[-\frac{\alpha^2}{\sqrt{V_0/E_R}}\right]. \quad (11)$$

The kinetic energy coupling in the x direction J_x also decreases monotonically with V_0/E_R for sufficiently large values [16] as described by
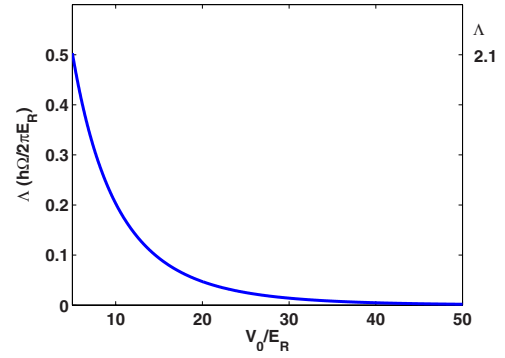
IX. SUMMARY

This paper discusses spectral and transport properties of the cold atom analog of a 2DEG in a lattice, subject to a non-Abelian gauge field with U(2) symmetry. In the continuum limit of the lattice, the system maps onto two oppositely charged coupled harmonic oscillators, with a coupling constant proportional to the strength of the non-Abelian field. The Landau energy levels of the Abelian problem evolve into entangled states of this particle-hole pair.

These features also characterize the energy spectrum of the corresponding lattice problem. In fact, the transition from Landau levels to Landau bands is the analog of the generalization from the butterfly to the moth spectrum as the Abelian system becomes non-Abelian. The non-Abelian coupling breaks the degeneracy of the Landau levels; the spectrum depends explicitly on the transverse momentum.

The non-Abelian system exhibits antiferrimagnetic-type ground states, whose components A and B, need not be degenerate, and in fact may have very different transport properties. A particularly interesting example of this is the zero-energy state for $\alpha_2 = 1/4$, where the degenerate A and B components have different localization properties. Additionally, an intriguing relationship between the A and B components occurs for $\alpha_2 = \frac{1}{2}$, as these two components correspond to the positive and the negative energy states of the system. Such novelties may open new avenues for exploring frontiers of physics with cold atoms.

The use of ultracold atoms to simulate relativistic as well as nonrelativistic theories and study the effect of disorder is an exciting field of research. In a two-dimensional lattice subject to a non-Abelian gauge field, one can induce not only localization transitions, but also a transition from relativistic to nonrelativistic theory by tuning the lattice anisotropy. A well-known feature of the Dirac Hamiltonian is an extra term in the conductivity attributed to *Zitterbewegung* (ZB) [18] corresponding to interband transitions. It has been suggested that such a term is responsible for the finite conductivity of graphene described by a massless Dirac energy spectrum [18]. In other words, it is ZB that makes it impossible to localize relativistic particles, as it is connected with the uncertainty of the position of a relativistic quantum particle due to the creation of particle-antiparticle pairs. Therefore, the origin of delocalization characterizing the non-Abelian system that persists even for infinite disorder ($\Lambda \to \infty$) can be attributed to ZB.

The detection of relativistic particle and a transition from nonrelativistic to relativistic dispersion in cold atoms in optical lattices was recently discussed; it was shown that the relativistic dispersion can be detected using atomic density profiles as well as Bragg spectroscopy [12]. Our detailed study for various values of α_2 captures some of the universal features of non-Abelian systems. Exploration of the two-dimensional space (α_1, α_2) may reveal additional phenomena, and the richness of U(N) gauge systems with $N > 2$ remains to be explored. Moreover, the effects of interparticle interactions remain to be investigated [19].

[1] J. Ruseckas, G. Juzeliunas, P. Ohberg, and M. Fleischhauer, Phys. Rev. Lett. **95**, 010404 (2005).

[2] D. Jaksch and P. Zoller, New J. Phys. **5**, 56 (2003).

[3] K. Osterloh, M. Baig, L. Santos, P. Zoller, and M. Lewenstein, Phys. Rev. Lett. **95**, 010403 (2005).

[4] D. R. Hofstadter, Phys. Rev. B **14**, 2239 (1976).

[5] E. J. Mueller, Phys. Rev. A **70**, 041603(R) (2004).

[6] N. Goldman and P. Gaspard, Europhys. Lett. **78**, 60001 (2007).

[7] R. Prange, in *The Quantum Hall Effect*, edited by R. Prange and S. Girvin (Springer-Verlag, Berlin, 1990).

[8] L. Onsanger, Philos. Mag. **43**, 1006 (1952).

[9] P. G. Harper, Proc. Phys. Soc., London, Sect. A **68**, 879 (1955); S. Aubry and G. Andre, Ann. Isr. Phys. Soc. **3**, 133 (1980).

[10] K. Drese and M. Holthaus, Phys. Rev. Lett. **78**, 2932 (1997).

[11] I. I. Satija, D. C. Dakin, and C. W. Clark, Phys. Rev. Lett. **97**, 216401 (2006); **98**, 269904(E) (2007).

[12] S.-L. Zhu, B. Wang, and L. M. Duan, Phys. Rev. Lett. **98**, 260402 (2007).

[13] L. Balents and M. P. A. Fisher, Phys. Rev. B **56**, 12970 (1997).

[14] For a review, see J. B. Sokoloff, Phys. Rep. **126**, 189 (1985).

[15] A. Jazaeri and I. I. Satija, Phys. Rev. E **63**, 036222 (2001).

[16] A. M. Rey, G. Pupillo, C. W. Clark, and C. J. Williams, Phys. Rev. A **72**, 033616 (2005).

[17] D. A. Steck data available at http://steck.us/alkalidata

[18] M. I. Katsnelson, e-print arXiv:cond-mat/0512337).

[19] N. Goldman, Europhys. Lett. **80**, 20001 (2007).